# Pitch and Torque Control to Maximize Wind Turbine Power Output in Partial Load Region

A Qualification Prospectus for

the Doctor of Philosophy Degree

by

Olgu Tanriverdi

Thesis Adviser A.V. Balakrishnan

Electrical Engineering Department

University of California, Los Angeles

May 2005

# Contents

# List of Figures

# List of Tables

# Abstract

Owing to concern over the high energy prices, there is much interest in renewable sources of electrical power generation, of which one of the most promising is wind power. With increasing wind energy production, demands to achieve better performance from wind turbines are growing. The challenge lies in developing a control algorithm that enables the turbine to operate continuously at the tip speed ratio that maximizes the rotor power coefficient, $C_p$, during wind speed variations in the partial load region.

In this thesis, we aim to deal with improvements of turbine performance via pitch and generator torque controls in the partial load region. Even though it is not possible to operate continuously at maximum efficiency due to large inertia of wind turbines, improvements in energy capture during variable speed operation can be gained by improved tracking of maximum power coefficient, $C_{po}$. We present a model for turbine dynamics based on a widely used drive train equation. In the model, we derived $C_p$ as a function of wind speed, rotor angular velocity, and blade pitch angle based on minimizing unconstrained least squares fit error. The $C_p$ data for the CART, one of the essential elements in calculation of the aerodynamic torque, are calculated by aerodynamic modeling softwares such as PROP or SymDyn. Then we argue that with the $C_p$ surface, depending on the operating point of the turbine, we can collectively apply pitch and generator torque controls to track the optimum tip-speed-ratio, $\lambda_o$, for a given wind speed and rotor angular velocity in the partial load region. In the tracking process, we keep the wind speed constant while updating the rotor angular velocity via generator torque to run the turbine at $C_{po}$. Moreover, for each rotor angular velocity, we also track the optimum blade pitch angle, $\beta_o$, via pitch control to stay on the optimum path to $C_{po}$.

Validation of our model was first done by inputting constant wind speeds with different initial rotor angular velocity conditions. For each initial value, the pitch angle and rotor angular velocity converged to their theoretical values. We also run the model without pitch control to illustrate the effect of the pitch control algorithm. Finally, we used the data of the Control Advance Research Turbine(CART) at National Renewable Energy Laboratory(NREL) to validate our simulation results. we input the four sets of 600 second real CART data to compare the outputs of the CART with the outputs of our simulation. In the simulation, we increased power output by between 4.16-20.33% compared to the real CART power output depending on the wind conditions.

# Chapter 1

# Introduction

Wind is an old established source of energy which is clean, renewable, abundant, and, in principle, accessible at no cost. A wind turbine is a device for extracting kinetic energy from the wind [2]. As one of the fastest growing energy sources worldwide, wind turbine energy is becoming more popular due to a growing deficit in the conventional source of energy. The installed wind power capacity in the world has been increasing at more than 25% per year for over last five years [3]. With increasing wind power production, the wind turbine industry has been challenged to produce wind turbines competitive in cost to traditional power sources, such as oil and coal. Therefore, the design of the control system and the dynamic component of wind turbine are growing research interests.

There are two kinds of wind turbines depending on their structures; horizontal axis wind turbine(HAWT) and vertical axis wind turbine(VAWT). Even though there are still some VAWTs, HAWTs are commonly used mainly because wind velocity increases at higher altitudes making HAWT more efficient. In horizontal axis category, there are two kinds of HAWTs; constant and variable speed wind turbines. Constant speed wind turbines is constrained to operate at a nearly constant speed and connected to

the utility grid directly without a converter. The power output of a wind turbine running at constant rotor speed is strongly governed by the chosen operational rotational speed. Performing well only in a chosen region makes constant speed turbines very inefficient. Conversely the variable speed wind turbines run at wide range of rotor and wind speeds making them more efficient. Since variable speed turbines operate at various rotor speeds, their power output is synchronized with the utility grid via converter. Due to their efficiency, variable speed wind turbines are preferred even though they require additional equipments like converter.

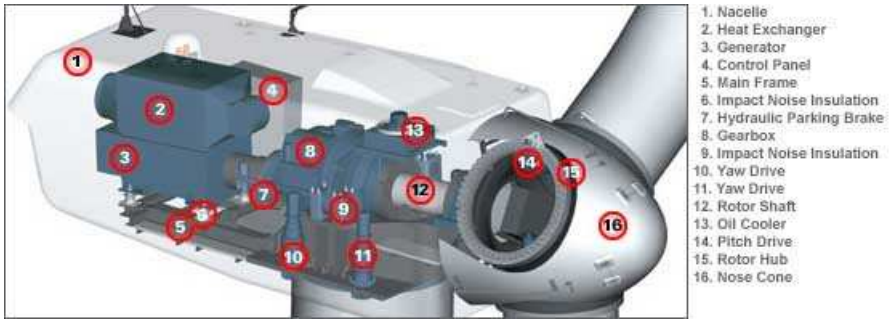


Figure 1.1: Horizontal axis wind turbine parts

The wind turbines consist of 6 main parts shown in Figure 1.1; Rotor, blades, drive-train, gearbox, converter, and generator. The rotor captures wind and generates the aerodynamic torque. Rotor then transfers the aerodynamic torque from high speed shaft to low speed shaft through gearbox and drive-train. Once the generator generates the power output, the converter synchronizes the power output with the grid and connects the generator output to the grid.

As seen in Figure 1.2, generally, there are three operation regions of wind turbines. The first region, where the wind speed is less than 5 m/s, the turbine runs at its start-up condition. In the second region, also called partial load region, where the wind speed varies between 5-11.5 m/s, the turbine runs below its maximum power limits. In this region, the pitch angle of the CART stays constant, and generator torque is used to capture the maximum available power. In the third region, full load region, where the wind speed is greater than 11.5 m/s, the turbine runs at right below its safe limits. In this region, pitch angle is changed via pitch control algorithm to feather and maintain its maximum power capture. In this thesis, the second region is our research interest.

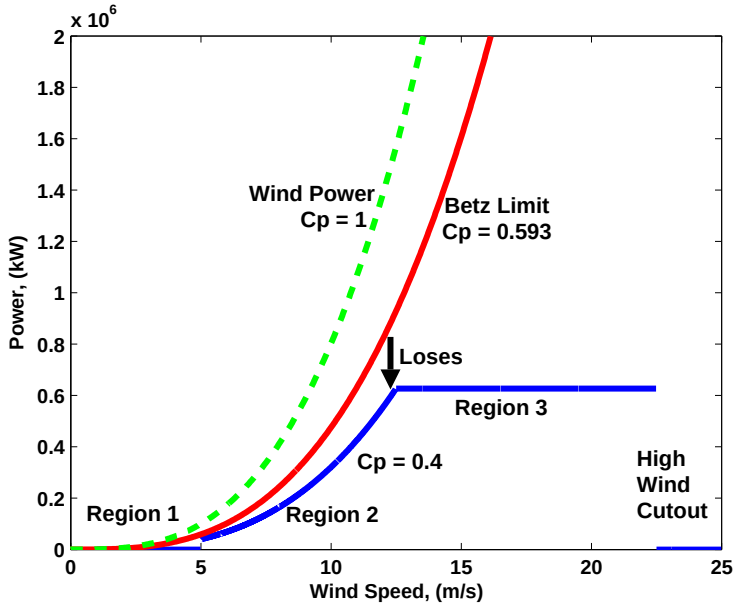


Figure 1.2: Power curves with operation regions

# Chapter 2

# Aerodynamics of Horizontal-axis Wind Turbines

## 2.1 Actuator Disc Model

The actuator disc model is the simplest model for wind turbines aerodynamics. The basic idea is that wind turbine extracts the kinetic energy from wind by removing some of its kinetic energy. The wind must slow down but only that the affected mass of air which passes through the rotor disc. As the air passes through the rotor disc, there is a drop in static pressure. This can be explained by stream tube. Since upstream of the stream tube has a cross sectional area smaller than that of the disc and an area larger than the disc downstream as seen in Figure 2.1, the similar pressure drop occurs for air passing through a stream tube.

We here note that the actuator disc theory applies based on the following assumptions [11].

1. Steady, homogenous wind
2. No obstruction to wind flow either upstream or downstream

3. Uniform flow velocity at disc

4. Wind flow passing through disc separable from remaining flow by well defined stream tube

5. Wind flow incompressible

6. Rotation of flow produced by disc

### 2.1.1 Momentum Theory

The mass of air which passes through a given cross section of the stream tube in a unit length of time is $\rho$AU, where $\rho$ is the air density, A is the cross sectional area, and U is the flow velocity. The mass flow rate must be the same everywhere along the stream tube;

$$\rho A_\infty U_\infty = \rho A_d U_d = \rho A_w U_w \tag{2.1}$$

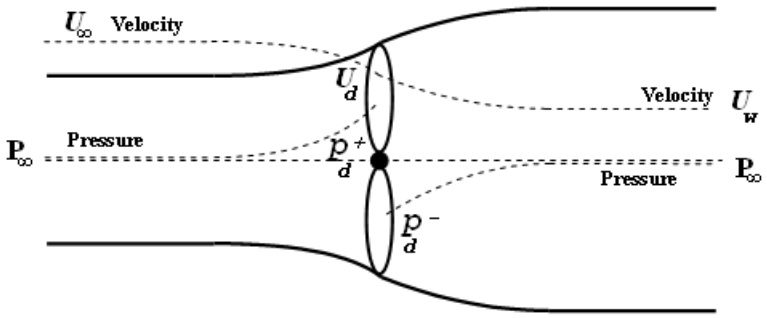


Figure 2.1: Actuator disc concept

The stream component of the induced flow at the disc is given by $-aU_\infty$, where $a$ is called the axial flow induction factor or the inflow factor. At the disc, therefore, the net stream velocity is

$$U_d = U_\infty(1-a) \tag{2.2}$$

The rate of change of momentum is equal to the overall change of velocity times the mass flow rate:

$$(U_\infty - U_w)\rho A_d U_d \tag{2.3}$$

The force causing this change of momentum comes entirely from the pressure difference across the actuator disc. Therefore,

$$(P_d^+ - P_d^-)A_d = (U_\infty - U_w)\rho A_d U_\infty(1-a) \tag{2.4}$$

To obtain the pressure difference $(P_d^+ - P_d^-)$ Bernoulli's equation is applied separately to the upstream and downstream sections of the stream tube. Bernoulli's equation states that under steady state conditions if no work is done on or by the fluid, the total energy in the flow remains constant. Thus, for a unit volume of air,

$$\frac{1}{2}\rho U^2 + P + \rho g h = \text{constant.} \tag{2.5}$$

Upstream, therefore, we have

$$\frac{1}{2}\rho_\infty U_\infty^2 + P_\infty + \rho_\infty g h_\infty = \frac{1}{2}\rho_d U_d^2 + P_d^+ + \rho_d g h_d \tag{2.6}$$

Assuming the flow to be incompressible ($\rho_\infty = \rho_d$) and horizontal ($h_\infty = h_d$) then,

$$\frac{1}{2}\rho U_\infty^2 + P_\infty = \frac{1}{2}\rho U_d^2 + P_d^+ \tag{2.7}$$

Similarly, downstream,

$$\frac{1}{2}\rho U_w^2 + P_\infty = \frac{1}{2}\rho U_d^2 + P_d^- \tag{2.8}$$

Subtracting equation (2.8) from equation (2.7)

$$(P_d^+ - P_d^-) = \frac{1}{2}\rho(U_\infty^2 - U_w^2) \tag{2.9}$$

Equation (2.4) then gives

$$\frac{1}{2}\rho(U_\infty^2 - U_w^2)A_d = (U_\infty - U_w)\rho A_d U_\infty(1-a) \tag{2.10}$$

and so

$$U_w = (1-2a)U_\infty \tag{2.11}$$

### 2.1.2 The Betz limit

The Betz limit gives us the maximum achievable value of the power coefficient by showing the maximum theoretical power that can be extracted from the wind by reducing its velocity.

The force on the air from equation (2.4)

$$F = (P_d^+ - P_d^-)A_d = 2\rho A_d U_\infty^2 a(1-a) \tag{2.12}$$

Hence the power extraction from the air is given by

$$Power = FU_d = 2\rho A_d U_\infty^3 a(1-a)^2 \tag{2.13}$$

A *power coefficient* is then defined as

$$C_p = \frac{Power}{\frac{1}{2}\rho U_\infty^3 A_d} \tag{2.14}$$

Therefore,

$$C_p = 4a(1-a)^2 \tag{2.15}$$

The maximum value of $C_p$ occurs when

$$\frac{dC_p}{da} = 4(1-a)(1-3a) = 0 \tag{2.16}$$

which gives us $a = \frac{1}{3}$, hence

$$C_{p_{max}} = \frac{16}{27} = 0.593 \tag{2.17}$$

We here note that for $a = \frac{1}{3}$, wake velocity given by equation (2.11) becomes $U_w = \frac{U_\infty}{3}$ showing how wind decelerates in the far wake. Also for $a \geq \frac{1}{2}$, wake velocity becomes zero or negative; therefore, momentum theory, as described, can not apply.

## 2.2 Blade Element Momentum (BEM) Theory

It is assumed that the forces on a blade element can be calculated by means of two dimensional aerofoil characteristics using an angle of attack. The angle of attack is determined from the resultant relative velocity in the cross sectional plane of the element, and the velocity component in the span-wise direction is ignored. Three dimensional

effects are also ignored as shown in Figure 2.2. The two dimensional forces are lift and drag forces. Both forces are calculated via lift, $C_l$ , and drag, $C_d$ , coefficients. Having information about how the airfoil characteristic coefficients $C_l$ and $C_d$ vary with the angle of attack, the forces on the blades for given values of $a$ and $a^{'}$ , tangential flow induction factor, can be determined.

From Figure 2.2, the relative velocity at the blade is

$$W = \sqrt{U_\infty^2(1-a)^2 + \Omega^2 r^2(1+a')^2} \tag{2.18}$$

which acts at an angle $\phi$ to the plane of rotation, such that

$$sin\phi = \frac{U_\infty(1-a)}{W} \quad \text{and} \quad cos\phi = \frac{\Omega r(1+a^{'})}{W} \tag{2.19}$$

The angle of attack $\alpha$ is given by

$$\alpha = \phi - \beta \tag{2.20}$$

The lift force on a span-wise length $r$ of each blade, normal to the direction of W, is therefore

$$L = \frac{1}{2}\rho W^2 c C_l r \tag{2.21}$$

and the drag force parallel to W is

$$D = \frac{1}{2}\rho W^2 c C_d r \tag{2.22}$$

where c is the chord length of blades.

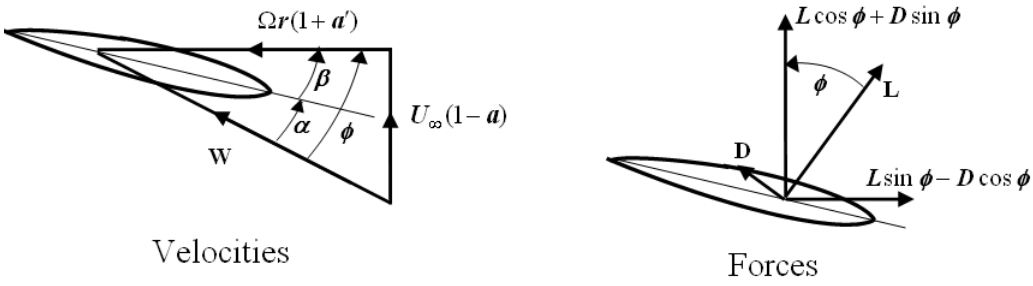


Figure 2.2: Rotor blade theory, velocities and forces

From $F_Q = Lsin\phi - Dcos\phi$ , the total useful torque that makes the rotor spin is

$$dQ = \frac{1}{2}\rho W^2 c(C_l sin\phi - C_d cos\phi)Ndr \tag{2.23}$$

where N is the number of blades. From $F_T = Lcos\phi + Dsin\phi$ , the total trust torque that puts load on the rotor is

$$dT = \frac{1}{2}\rho W^2 c(C_l cos\phi + C_d sin\phi)Ndr \tag{2.24}$$

and the power is

$$dP = \Omega dQ = \frac{1}{2}\rho\Omega W^2 c(C_l sin\phi - C_d cos\phi)Ndr \tag{2.25}$$

Modeling the rotor and calculating the aerodynamic torque and power via using blade element theory has; however, a number of drawbacks [15].

- Instead of only one wind speed signal, an array of wind speed signals has to be applied.
- Detailed information about the rotor geometry should be available.
- Computations become complicated and lengthy.

Rather equation (2.14) is used in calculation of the rotor aerodynamic torque and power.

# Chapter 3

# Literature Review

## 3.1 Aerodynamic Models Review

The fundamental analysis of the wind turbine rotor aerodynamics was originally developed by Betz [4]. The simple model was used to determine the power from an ideal turbine rotor. The model was based on a linear momentum theory to predict the performance of ship propellers. The turbine is represented by a uniform "actuator disk" which creates a discontinuity of pressure in the stream tube of air flowing through it. Later, Prandtl [5] introduced a relatively simple method to estimate so-called tip correction factor. He considered the vortex sheets behind the turbine to be rigid planes moving with a velocity equal to the axial induced velocity. Later, annulus momentum vortex theory was proposed by Glauert [6, 7]. With this theory, each radial section of blade is analyzed independently using two-dimensional airfoil data and equations based upon continuity and conservation of momentum. Subsequently, Wilson and Lissaman [8] modified Glauert's angular momentum equations to include tip correction factor derived by Prandtl for wind turbine rotor. This work forms the basis on which most modern design tools have been constructed. Swalwell et al. [9, 10] Blade Element Theory (BEM) to predict the aerodynamic performance of Horizontal Axis Wind Turbine

(HAWT). It was shown that even turbines that pitch the blades to avoid stall do not avoid the extra load, as the pitching mechanisms are too slow to avoid stall conditions during wind gusts. It was suggested that the predictions of the BEM method with high angle of attacks may be improved by accounting for the effects of turbulence on performance.

## 3.2 Constant Speed Wind Turbine Review

At the beginning, applying controllers to wind turbine was not a concern. They operate at fixed pitch angle and constant rotational speed. Safety margins were large, disabling wind turbines to capture more available power [11]. Later, stall was used to regulate the blades angle in the case of excessive power [12]. However, the performance of stall regulated rotor was satisfactory as blade stalls, but blades were under big drag forces putting them under large thrust loads.

## 3.3 Variable Speed Wind Turbine Review

As the problems with wind turbines becomes clearer, more control algorithms have been approached. At the same time, the demand for variable speed turbines increased due to their ability to capture more energy for a large range of wind speed. Muljadi et al. [13] used a model from turbine drive train and aerodynamic torque equations for the variable speed wind turbines. Pitch control was kept at its optimum operation according to the wind turbine power coefficient curve to maximize the power capture. Different pitch acceleration rates were used to see its power out effects. Moriarty et al. [14] used PID controller to reduce output power fluctuations and aerodynamic loads on the rotor. Also a scale study was performed to show that increasing rotor radius

by 50% more than doubled the rated power and annual energy capture. Slootweg et al. [15] used the numerical approximation to calculate the power coefficient for given tip-speed-ratio and the pitch angle. Rotor speed controller and pitch controller were derived to have the optimal energy capture. Hand et al. [16, 17] used PID controller to have a constant power production by using a linear and nonlinear model for variable speed wind turbines. The results for both models showed that power output changes depending on the operation point at which the system is linearized.

Moreover, Lima et al. [19] and Rocha [20] applied the $H_\infty$ loop shaping design methodology to controller design for variable speed stall regulated wind turbine. The main objective was to increase the efficiency on energy conversion reducing the detrimental dynamic loads due to wind fluctuation and ripple torque.

Novak et al. [21] linearized aerodynamic loads on the wind turbine to have a linear model. Linear model was used to improve the energy capture. In designing LQG controller, he used generator speed and generator torque for the measured output and the input signal, respectively. He also derived nonlinear model based on actuator disk model and compared them with linear models. Ma [22] derived linear and nonlinear models for wind turbine by using drive train equations and aerodynamic forces on rotor blades. Then he applied adaptive extremum and LQG control algorithms to his model. Connor et al. [23] applied an LQG controller, only active in full load region, to a constant speed horizontal axis wind turbine via pitch of the rotor blades. He showed that the output power of his non-linear model turbine can be kept rated for above rated wind speed and in the presents of wind gusts. Subsequently, Stol [24] in his Ph.D. thesis gives a general view of wind turbines including linear and nonlinear modeling, linearization, state-space model, LQG controller in the application of yaw and pitch alignments, and computer code simulations. For the computer simulation, linear state-space model with multiple degree of freedom was developed. He basically

used active feedback control theory to apply pitch control for power regulation.

## 3.4 NREL Review

The main contributor of my thesis, Johnson et al. [1, 26, 27] looked into modeling and control strategies of variable speed wind turbines specifically the CART at NREL in the partial load region. A simple drive train equation was used in the modeling and applied the standard $k\omega^2$ torque control with fixed pitch angle in the partial load region. It was showed that even if the value of k is set at the perfect value in the variable control algorithm, it is was not very efficient enough to capture all available wind power. The adaptive torque control algorithm was applied in which k is updated by comparing the averages of the previous turbine power output with the current power output. However, since the update of k only depends on the previous power outputs, the controller does not check to see whether or not the turbine runs in its optimum operating point. In addition, due to the fact that the pitch angle is kept constant in the second region, it is not expected to run the wind turbine at its optimum operating point in the second region.

Pierce [18] applied the estimation and control theories to a linear state space model that he derived by linearizing drive train equations. Blade pitch is included in the observer to estimate the effects of changing wind speed, and at the end, he used computer codes to evaluate the validity of his model. Four different control algorithms were implemented, including standard $k\omega^2$ torque control to compare the results. The increase in produced energy ranged from 1.26% to 3.75% depending on the wind speed and the control method used. It was concluded that using blade pitch control is a good way to increase energy capture.

## 3.5 Our Contribution

While the existing results concerning performance of variable speed wind turbines are encouraging, modeling and the control issues in the partial load region still need to be addressed more. With a fixed angle without any pitch control, it is not likely to capture the maximum available energy in the partial load region due to the variation in the wind. Since the wind speed and tip speed ratio are constantly changing in the partial load region, we can not expect wind turbine to run at its optimum operating point with a fixed pitch angle. Another important issue is that generally pitch control is only used for feather effects to limit the power output in full load region, not used to track the optimum operating point in the partial load region. In our control strategy, pitch control has a great effect on running the turbine at its optimum operating point. Moreover, in general, updating the generator torque is done by averaging previous power outputs regardless of whether or not the turbine runs at $C_{po}$; whereas, in our control algorithm, it is done based on enforcing the turbine to operate at $C_{po}$ regardless of previous power conditions.

It is our goal to apply pitch and generator torque controls simultaneously to run the variable speed turbines at their optimum operating point in the partial load region.

# Chapter 4

# Definition of the problem

Our goal is to operate turbine at the optimum tip-speed-ratio that maximizes power capture for given wind speeds in the partial load region. We apply pitch and generator torque control to enforce the turbine to run at $C_{po}$. We developed our model and control algorithm based on the characteristics of the CART at NREL. The CART is a medium scale turbine that has been extensively modified to make it suitable for control testings, see table 4.1 [25].

The CART is currently using fixed pitch angle and not using any pitch control in the partial load region, where the wind speeds vary between 5-11.5 m/s. In addition, the adaptive torque control of the CART only depends on the average of the previous power outputs and the direction of the wind speed regardless of whether or not the turbine is operating at its optimum operating point, $C_{po}$. $C_{po}$ means that not only is the turbine running at its $\lambda_o$, but it also has the right blade pitch angle, $\beta_o$, to have $C_{po}$.

The originality of our work is that we apply adaptive pitch and generator torque control algorithms to run the turbine at its $C_{po}$ in the partial load region. Pitch angle and the generator torque are changed adaptively to track $C_{po}$ for given wind speeds.

Table 4.1: CART Capabilities

| | |
|---|---|
| Pitch system maximum speed | 19 ° per second |
| Generation system electrical power | 650 kW |
| Maximum rotor torque | 162 kNm at 41.7 RPM |
| Maximum rotor speed | 58 RPM |
| Yaw rate | 0.5 ° per second |
| Control system cycle time | 100ms |
| Data acquisition rate | 100Hz |

We first present a model for turbine dynamics based on widely used a drive train equation. The data for $C_p(v(t), \omega(t), \beta(t))$ , one of the essential elements in calculation of the aerodynamic torque, are derived by using modeling softwares such as PROP or SymDyn. We argue that $C_p$ can be written as a function of wind speed, rotor angular velocity, and pitch angle. After having the $C_p$ surface, depending on the operating point of the turbine, we apply pitch and generator torque control to track the optimum operating point, $C_{po}$, for a given wind speed and rotor angular velocity. In the tracking process, we keep the wind speed constant while updating the rotor angular velocity via generator torque to run the turbine at $C_{po}$. Moreover, for each rotor angular velocity, we also track the optimum pitch angle via pitch control to stay on the optimum path to $C_{po}$.

## 4.1 Formulation of the Problem

We start the formulation with a widely used drive train equation

$$J\frac{d\omega(t)}{dt} = Q_A(t) - Q_G(t) \tag{4.1}$$

where the value of the rotor inertia is given by

$$J = 388500 \quad kg.m^2 \tag{4.2}$$

The aerodynamic torque on the rotor induced by wind

$$Q_A(t) = a_k C_p(v(t), \omega(t), \beta(t))\frac{v(t)^3}{\omega(t)} \quad N.m \tag{4.3}$$

where the value of $a_k$ is given by

$$a_k = \frac{1}{2}\rho\pi r^2 = 901.9 \quad kg/m \tag{4.4}$$

where $r = 21.65\ m$ is the radius of the rotor of the CART and $\rho = 1.225\ kg/m^3$ is the air density. Then, we write the generator torque, one of our control inputs,

$$Q_G(t) = k(t)\omega(t)^2 \quad N.m \tag{4.5}$$

where $k(t)$ is a parameter used in the torque control. $v(t)$ is the wind speed in m/s, $\omega(t)$ is the angular velocity in rad/s, and $\beta(t)$ is the pitch angle, in degrees. $\beta(t)$ is the angle measured between the aerofoil zero lift line and the plane of the disc.

Our main wind turbine equations are:

$$\frac{d\omega(t)}{dt} = f(v(t), \omega(t), \beta(t), k(t)) \tag{4.6}$$

where

$$f(v(t),\omega(t),\beta(t),k(t)) = \frac{1}{J}\Big(a_k C_p(v(t),\omega(t),\beta(t))\frac{v(t)^3}{\omega(t)} - k(t)\omega(t)^2\Big) \tag{4.7}$$

and the dynamics of the pitch actuator with reference pitch input $\beta_{ref}(t)$

$$\frac{d\beta(t)}{dt} = -m\beta(t) + m\beta_{ref}(t) \tag{4.8}$$

where $m > 0$.

## 4.2 Pitch Drive System

The dynamics of the pitch actuators is modeled as a first order low pass filter with DC gain of 1 and a time constant of 1/m second in equation (4.8). Moreover, we determine the value of $m > 0$ by using one of the specifications of the pitch drive system of the CART, see Table 4.1; the maximum pitch speed of the actuators is $19\,^\circ$ per second.

We need to have $m > 0$ such that we have

$$\Big|\frac{d\beta(t)}{dt}\Big| \leq 19\,^\circ \quad \forall\ t > 0 \tag{4.9}$$

First we write $\beta(t)$ with initial condition $t = t_1$;

$$\beta(t) = \beta(t_1)e^{-m(t-t_1)} + \int_{t_1}^{t} e^{-m(t-s)} m\beta_{ref}(s)ds \quad \forall\ t > t_1 \tag{4.10}$$

where $\beta_{ref}(s)$ is a constant $\forall\ s\ \in [t_1, t]$ and $(t - t_1) = 1$.

Since we must satisfy equation (4.9) $\forall\, m > 0$,

$$\Big|\frac{d\beta(t)}{dt}\Big| =$$

$$= \Big| - m\beta(t_1)e^{-m(t-t_1)} - \int_{t_1}^{t} e^{-m(t-s)}m^2\beta_{ref}ds + m\beta_{ref}\Big| \leq 19^\circ \quad \forall\, t > t_1 \tag{4.11}$$

$$= \Big| - m\beta(t_1)e^{-m(t-t_1)} - m\beta_{ref}e^{-mt}\Big(e^{ms}\Big|_{t_1}^{t}\Big) + m\beta_{ref}\Big| \leq 19^\circ \quad \forall\, t > t_1 \tag{4.12}$$

$$= \Big|me^{-m}\Big(\beta_{ref} - \beta(t_1)\Big)\Big| \leq 19^\circ \quad \forall\, m > 0 \tag{4.13}$$

$$= \Big|m\Big(\beta_{ref} - \beta(t_1)\Big)\Big| \leq 19^\circ \quad \forall\, m > 0 \tag{4.14}$$

$$\Big|\beta_{ref} - \beta(t_1)\Big| \leq 35^\circ \quad \forall\, m > 0 \quad \Rightarrow \tag{4.15}$$

$$0 < m \leq \frac{19}{35} \tag{4.16}$$

$\forall\, m \leq \frac{19}{35}$ , the maximum pitch speed of the actuators is less than 19 degrees,

Indeed we can find the same result by using;

$$\Big|\frac{d\beta(t)}{dt}\Big| = \Big| - m\beta(t) + m\beta_{ref}(t)\Big| \leq 19^\circ \quad \forall\, t > 0 \tag{4.17}$$

and the equation (4.15).

To illustrate the performance of the pitch actuators with $m = \frac{19}{35}$ , we input $\beta_{ref} = 35^\circ$ as the input of the pitch drive system in equation (4.8). As shown in Figure 4.1, the maximum pitch speed of the pitch drive system is less than $19^\circ$ per second, the actuators can not track $19^\circ$ per second.

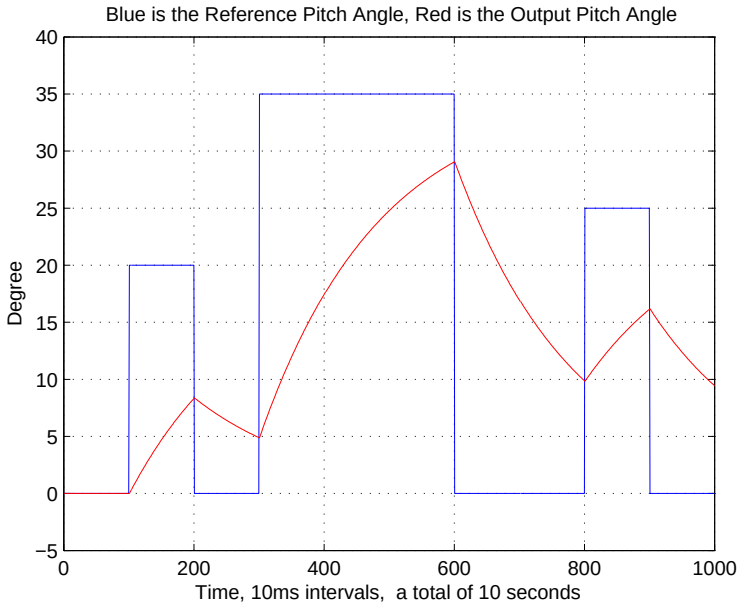


Figure 4.1: Acceleration rate of pitch controller

## 4.3 Derivation of the Rotor Power Coefficient

The $C_p(\lambda(t), \beta(t))$ data for the CART at NREL are derived by aerodynamic modeling softwares such as PROP or SymDyn. As seen in Figure 4.2, the data of the power coefficient have 27 $\lambda(t)$ values between [1,14] and 36 $\beta(t)$ values between [-5,30].

By using the data, we interpolate $Cp(\lambda(t), \beta(t))$ as a 9th degree polynomial of $\lambda(t)$ and $\beta(t)$ in equation (4.18). The total of 54 coefficients are found by using unconstrained least square minimization method. As seen in the Figure 4.3, least mean square error

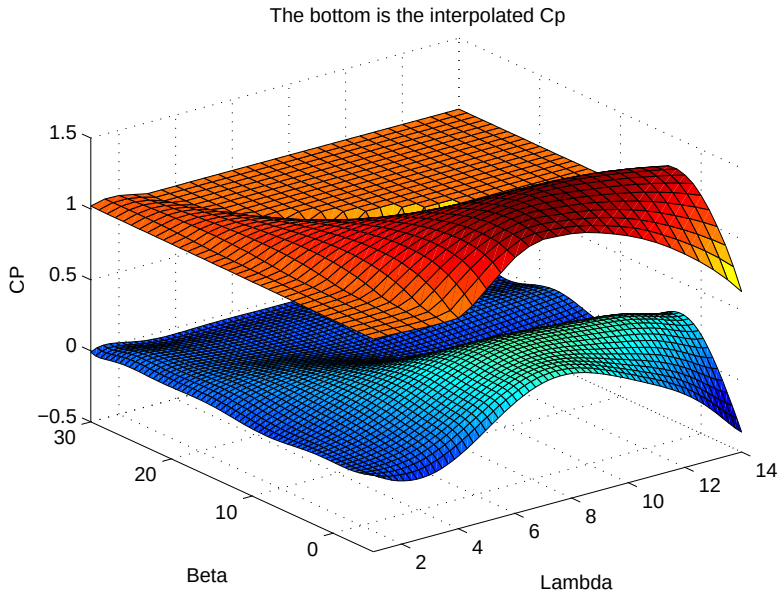


Figure 4.2: 3D plot of $C_p(\lambda(t), \beta(t))$ as a function of $\lambda(t)$ and $\beta(t)$

function is a convex function in polynomial degrees, and the 9th degree polynomial approximation gives us the lowest least mean square error.

$$C_p(\lambda(t), \beta(t)) = \sum_{m=1}^{9} \sum_{n=0}^{m} \mathbf{c}_{m+n} \lambda(t)^{m-n} \beta(t)^n \tag{4.18}$$

From the data, $C_p(\lambda(t), \beta(t))$ polynomial has 27x36=972 values corresponding to 27 $\lambda(t)$ and 36 $\beta(t)$ values. So the problem is to find 54 unknown polynomial coefficients, $\mathbf{c}_i$ , by solving the unconstrained least square minimization problem in equation (4.19).

$$\min_{\mathbf{c}} \|C_p(\lambda(t), \beta(t)) - b\|^2 = \min_{\mathbf{c}} \|A\mathbf{c} - b\|^2 = \min_{\mathbf{c}} \sum_{n=1}^{972} (a_n \mathbf{c} - b)^2 \tag{4.19}$$

where A is a 972 by 54 matrix, b is a 972 by 1 vector, and $\mathbf{c}$ is a 54 by 1 vector that has the 54 unknown coefficients.

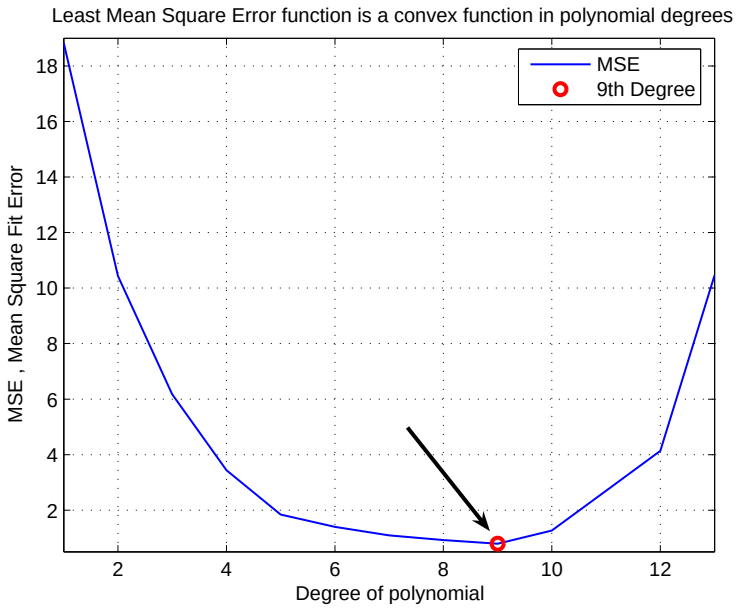


Figure 4.3: $C_p(\lambda(t), \beta(t))$ approximation by least mean square error

We solve the unconstrained minimization problem for $\mathbf{c}$ to find the 54 unknown coefficients. We will later use the interpolated $C_p(\lambda(t), \beta(t))$ function in linearization process of the system around its operation point.

## 4.4 Effects of k(t) in the Torque Control to the System

In order to illustrate the effects of $k(t)$, one of our control inputs, to the system better, we plot $f(v(t), \omega(t), \beta(t), k(t))$. As shown in Figure 4.4 , for fixed $v(t) = r$ and $\beta(t) = 1^\circ$ values, by changing the values of $k(t)$, we obtain the desired rotor angular velocity to track $\lambda_o$. This is the main idea behind improved energy capture from variable speed operation; however, this goal is only partially achievable due to rapid variations in wind speed and the large inertia of the wind turbine rotor.

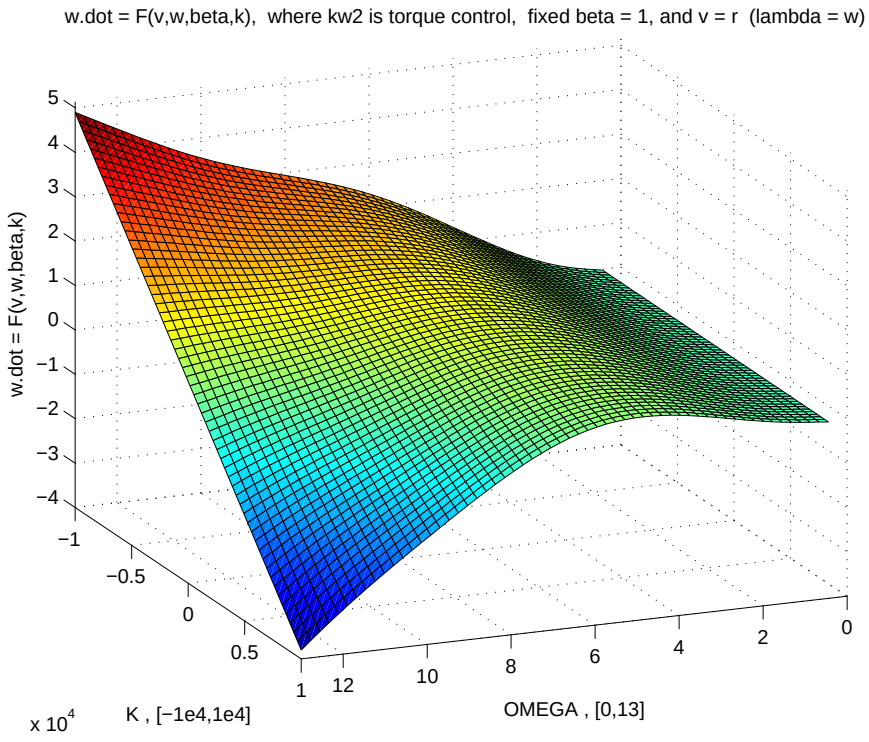


Figure 4.4: $\frac{d\omega(t)}{dt} = F(v(t), \omega(t), \beta(t), k(t))$ , fixed $\beta(t) = 1\,^{\circ}$, and $v(t) = r$

## 4.5 Illustration of Some CART data from NREL

The Figure 4.5 shows an interval of 60,000 samples, equivalent of 10 minutes data from the CART, with sampling rate of 100Hz. Due to the value difference, we scaled the power by 1/70 to be able to plot all variables in the same plot. We here see that there is a strong correlation among wind speed, power output, angular velocity, and torque. We also note that torque control is applied to track the desired angular velocity in the partial load region. In the full load region, $\omega(t)$ is limited to 4.37 rad/s to limit the power output.

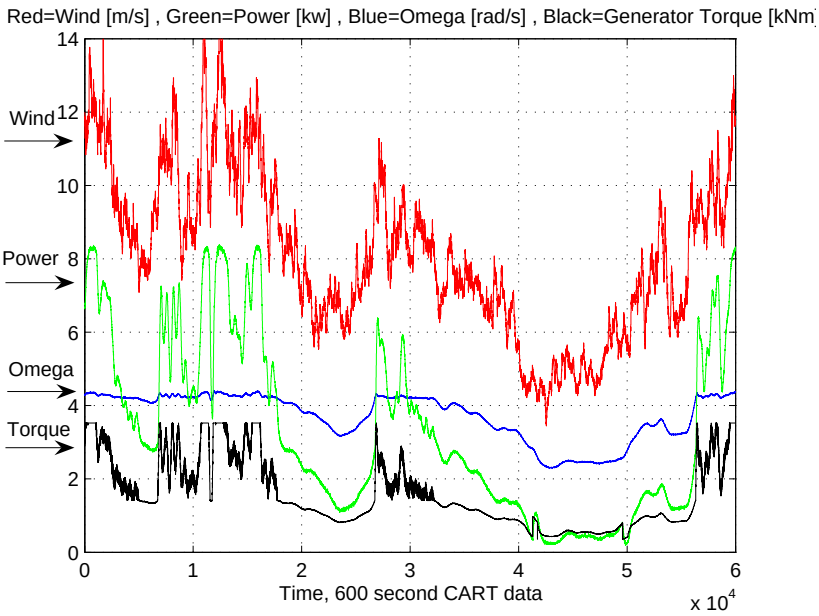


Figure 4.5: Illustration of some CART data

# Chapter 5

# Control Algorithm

We utilized the Simulink from Matlab 7.0 R14 to implement our model in the simulation as shown figure 5.1. We input wind speed, reference pitch angle, and generator torque to our model as our inputs, and we observe the generated power, rotor angular velocity, and actual pitch angle as our outputs. In the modeling, we used the specifications of the CART. We used the data of the CART rotor power coefficient, $C_p(v(t), \omega(t), \beta(t))$, derived from PROP, an aerodynamic modeling software. Moreover, wind speed direction is assumed to be perpendicular to the rotor all the time in the simulation, no yaw control. We run the simulation with 10ms time intervals since all data we have from the CART were sampled at 100 Hz. Our model is run in the partial load region, where the wind speeds vary between 4-12 m/s. Pitch and torque control were applied to operate our model at its optimum tip-speed-ratio.

There are a total of four cases into which we looked. The first three cases, we used a constant wind speed of $v(t) = 10\,\mathrm{m/s}$ for the justification of our model and algorithm. Finally, to validate our model and the control algorithms, we input the real CART wind speed data to our simulation and compared our simulation outputs to the ones of the CART in the fourth case. The CART wind speed data used in the final case were

collected by an anemometer on the nacelle of the CART

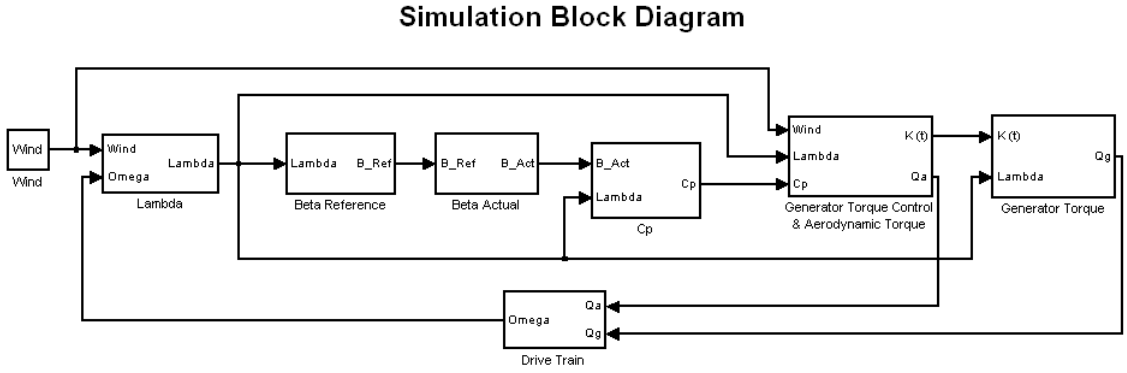


Figure 5.1: Simulink block diagram

## 5.1 Torque and Pitch Control

The control algorithms used in the simulation are based on torque and pitch control. We input constant wind speeds to our model for a certain period of time. During that period, we aim to reach the optimum operating point $C_{po} = 0.4292$. Once we reach $C_{po}$, turbine sustains its steady state operating point until the next constant wind speed.

For example, in the fourth case in Section 6.2, we input one averaged constant wind speed for each 10 second wind data. For each 10 second constant wind speed, we reach $C_{po}$ in the steady state. Keeping wind speed constant for 10 second does not affect the performance of the turbine much due to the large inertia of the rotor. Since we can not change the speed of the rotor as fast as wind changes, keeping wind speed constant for a while helps turbine track the steady state values. However, in our work, the main reason behind keeping the wind speed constant is that for each constant wind speed value, lambda becomes a linear function of omega, $\lambda(t) = \frac{\omega(t)r}{v}$. Then by applying the

generator torque control, we change the rotor speed to track the optimum tip-speed-ratio, $\lambda_o = 8.5$. Along with changes in the rotor angular velocity by torque control, we also apply the pitch control simultaneously by assigning beta value for each lambda to ensure that the turbine is operating its optimum point, $C_{po}$. As shown in Figure 5.2, for each lambda value, we have a reference pitch angle, $\beta_{ref}(t)$ that maximizes the $C_p(v, \omega(t), \beta(t))$. The effects of pitch control to the turbine's performance becomes more apparent in Section 6.1.

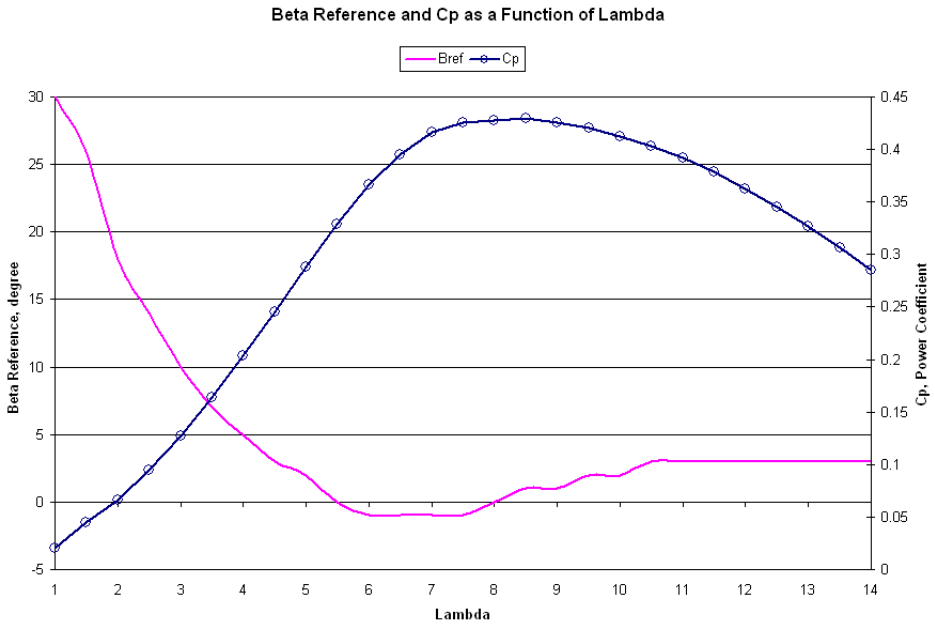


Figure 5.2: $\beta_{ref}(t)$ as a function of $\lambda(t)$

As seen in Figure 5.1, we obtain $\beta_{act}$ from the pitch drive system in the calculation of $C_p(v, \omega(t), \beta(t))$ to have the generated aerodynamic torque and power. The aerodynamic torque is given by

$$Q_A(t) = a_k \, C_p(v, \omega(t), \beta(t)) \frac{v^3}{\omega(t)} \tag{5.1}$$

and the generated power is

$$P_{out}(t) = Q_G(t)\omega(t) + J\omega(t)\frac{d\omega(t)}{dt}$$

$$= g(v, \omega(t), \beta(t))\omega(t)^3 \tag{5.2}$$

where

$$g(v, \omega(t), \beta(t)) = \frac{a_k r^3 C_p(v, \omega(t), \beta(t))}{\lambda(t)^3} \geq 0 \tag{5.3}$$

After having $C_p(v, \omega(t), \beta(t))$, by using equation (4.6), we have

$$\frac{\omega(t)}{dt} = \Big(\frac{g(v, \omega(t), \beta(t)) - k(t)}{J}\Big)\omega(t)^2 \tag{5.4}$$

In the generator torque control block, we accelerate or decelerate the rotor angular velocity to track $\lambda_o$ in the steady state by applying $k(t)$ to equation (5.4).

We have three instances to assign $k(t)$ in our control algorithm:

1. $k(t) = 0$ for $\lambda(t) < \lambda_o - \epsilon$
2. $k(t) = \frac{3g(v,\omega(t),\beta(t))}{2}$ for $\lambda(t) > \lambda_o + \epsilon$
3. $k(t) = g(v, \omega(t), \beta(t))$ for $\lambda_o - \epsilon \leq \lambda(t) \leq \lambda_o + \epsilon$ (steady state)

where $\epsilon = 0.001$ is the tolerance left and right side of the optimum tip-speed-ratio, $\lambda_o = 8.5$.

The strategy of assigning $k(t)$ comes from the fact that since power is proportional to the cube of wind, if there is any available wind, we would like rotor to capture all

available wind as much as possible. However, when wind decreases, it is not required to decrease the rotor velocity as fast since we have the kinetic energy of the rotor from the high wind, we decrease the rotor velocity more moderate. That is the reason the speed of increasing the rotor velocity is double of decreasing it. In the steady state instance, the turbine operates at $C_{po} = 0.4292$, there is no change in the rotor velocity.

# Chapter 6

# Simulation Results

## 6.1 Cases with a Constant Wind Speed

In this section, we run the simulation by inputting constant wind speed, $v(t) = 10\,\mathrm{m/s}$, to see whether or not rotor angular velocity, the pitch angle, and the tip-speed ratio would converge to their theoretical values. Moreover, additional to the torque control, to illustrate the effects of pitch control, we run the simulation with and without pitch control algorithm. The first two cases we run the simulation with a constant wind speed of $v(t) = 10\,\mathrm{m/s}$ for 25 seconds and 30 seconds, equivalent of 2500 and 3000 iterations by giving two different initial rotor speeds, $\omega_{initial}(t) = 1\,\mathrm{rad/s}$ and $\omega_{initial}(t) = 6$ rad/s respectively. For the third case, we run the simulation for 80 seconds due to low initial rotor velocity $\omega_{initial}(t) = 0.1$ rad/s. For all cases, we track $C_{po} = 0.4292$ , the optimum value of $C_p(v(t), \omega(t), \beta(t))$ in the algorithm. $C_{po}$ is acquired when we have $\beta_o = 1\,^\circ$ and $\lambda_o = 8.5$.

### 6.1.1 Case I, $\omega_{initial}(t) = 1$ rad/s

We start the simulation with $\omega_{initial}(t) = 1$ rad/s with constant wind speed, $v(t) = 10$ m/s which gives us $\lambda_{initial}(t) = 2.165 < \lambda_o = 8.5$. As shown in Figure 6.1, $\omega(t)$ increases to track $\omega(t) = 3.926$ corresponding to $\lambda_o = 8.5$. Since the wind speed is constant, increase in $\omega(t)$ is moderate. As we see in case IV, for increasing wind speeds, the increase in $\omega(t)$ would be sharper. We also emphasize the difference when no pitch control is applied. As seen in the Figure 6.1, pitch control changes $\beta(t)$ as $\omega(t)$ changes to track $C_{po}$ faster. When the pitch control is not used, it takes longer to reach $C_{po}$ causing the power loses. Moreover, it takes 12 seconds to have the steady state values with pitch control and 15 seconds without pitch control. This example clearly illustrates the importance of the pitch control in the partial load region.

### 6.1.2 Case II, $\omega_{initial}(t) = 6$ rad/s

In Case II, $\omega_{initial}(t) = 6$ rad/s with constant wind speed again, $v(t) = 10$ m/s which gives us $\lambda_{initial}(t) = 13 > \lambda_o = 8.5$. As shown in Figure 6.1, $\omega(t)$ decreases to track $\omega(t) = 3.926$ corresponding to $\lambda_o = 8.5$. As in Case I, decrease in $\omega(t)$ is moderate. $\beta(t)$ also changes as $\omega(t)$ changes to track $C_{po}$. It takes 23 second to have the steady state values, much longer than Case I due to assigning strategy of $k(t)$ explained in Section 5.1.

### 6.1.3 Case III, $\omega_{initial}(t) = 0.1$ rad/s

In this case, we run the simulation with and without pitch control to illustrate the difference. In no pitch control case, pitch angle is fixed, $\beta(t) = 1\,^\circ$. Moreover, in this section, we start from almost a start-up condition, where $\omega_{initial}(t) = 0.1$ rad/s/ which gives us $\lambda_{initial}(t) = 0.2165 < \lambda_o = 8.5$. Due to the large inertia of the turbine rotor, it takes 54 seconds to converge the steady state values. As shown in Figure 6.3, we first would like to emphasize the big difference in the generated power between with and

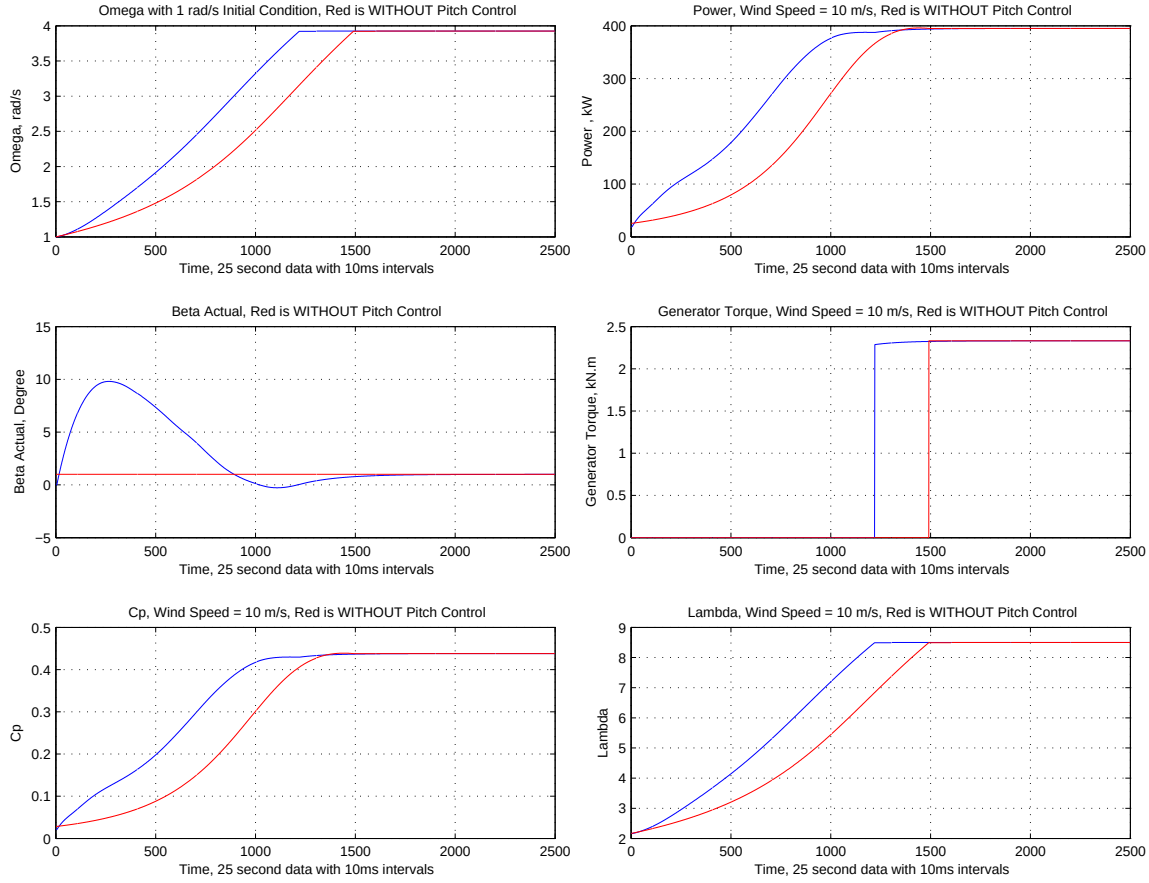


Figure 6.1: Case I, constant wind speed, $v(t) = 10\,\mathrm{m/s}$ with $\omega_{initial}(t) = 1$ rad/s initial condition, red is without pitch control

without pitch control. With pitch control, the first 40 seconds, $\omega(t)$ increases slowly and reaches around $\omega(t) = 0.5$. The later 14 seconds, faster increase occurs as the kinetic energy of the rotor increases, the large rotor inertia loses its effect. We also note that pitch angle stays at $30\,^\circ$ for almost 30 seconds of the first 40 seconds to keep $C_p$ at its optimum values during the transaction to the steady state. However, without pitch control, it takes 185 seconds to reach the steady state values. Similarly, the first 155 seconds, $\omega(t)$ increases slowly and reaches around $\omega(t) = 0.5$. The later 30 seconds faster increase occurs. While with the pitch control, the power reaches 400 kW in 55

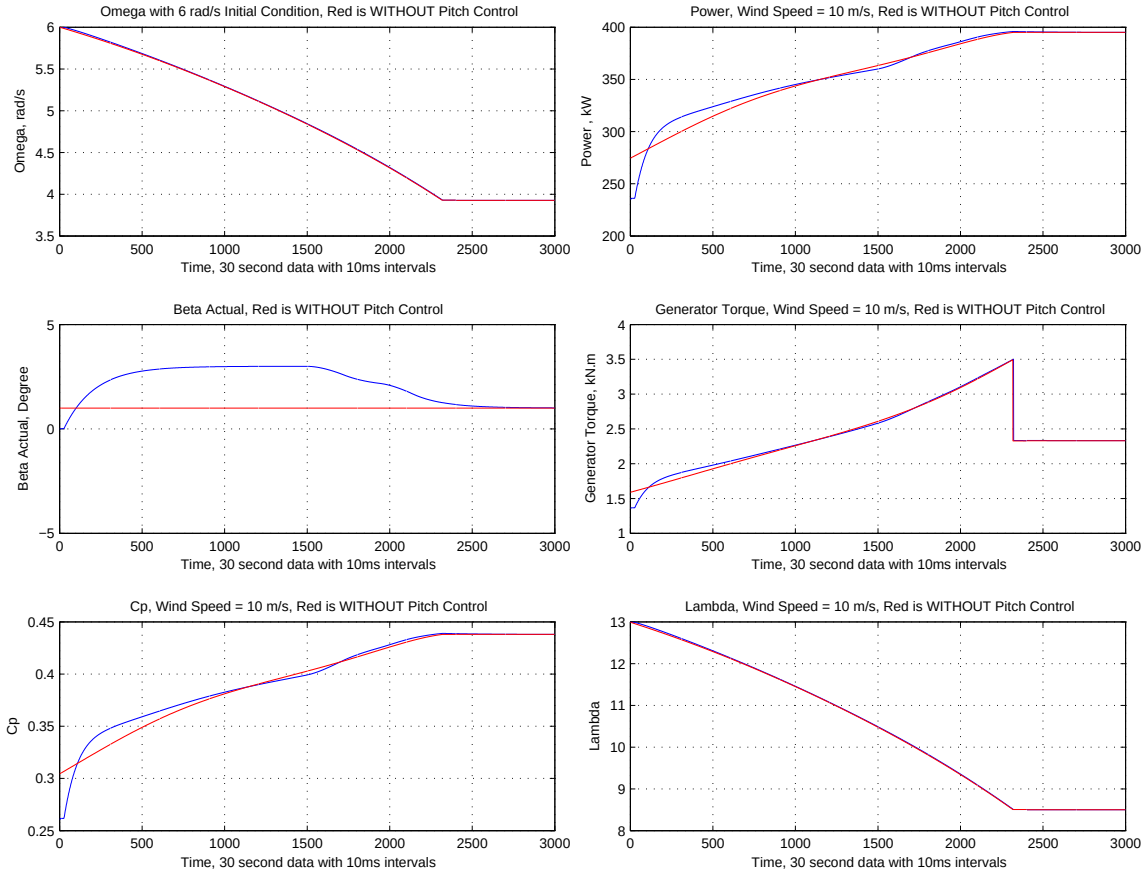


Figure 6.2: Case II, constant wind speed, $v(t) = 10\,\mathrm{m/s}$ with $\omega_{initial}(t) = 6$ rad/s initial condition, red is without pitch control

seconds, without pitch control, at the same time, the power is around 0.2 kW. This is only one of the many cases that illustrate how much power loses occur when no pitch control is applied in the partial load region.

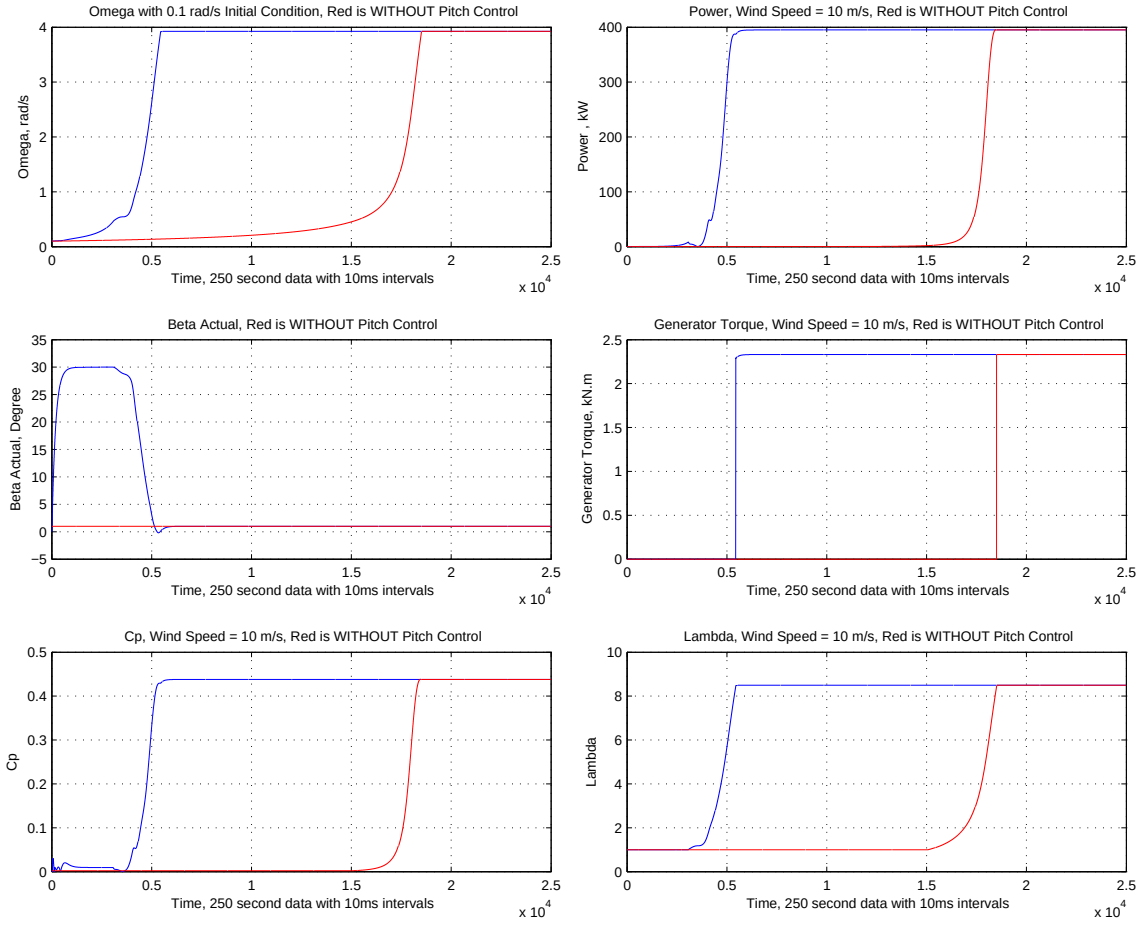


Figure 6.3: Case III, constant wind speed, $v(t) = 10\,\mathrm{m/s}$ with $\omega_{initial}(t) = 0.1$ rad/s initial condition, red is without pitch control

We here note that all three cases, the simulation ends with the steady state values of $\lambda_o = 8.5$ and $C_{po} = 0.4292$

## 6.2 Final Case, validation of the Model and Algorithm

For the fourth case, we input the real wind data to our model for 600 seconds of four sets of data. We use a constant wind speed for each 10 seconds that is equal to the